Bone Reports 20 (2024) 101748

Contents lists available at ScienceDirect

Bone Reports

journal homepage: www.elsevier.com/locate/bonr

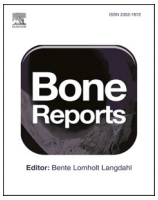

In vivo imaging of bone collagen dynamics in zebrafish

Hiromu Hino, Shigeru Kondo, Junpei Kuroda *

Graduate School of Frontier Biosciences, Osaka University, Suita, Japan

ARTICLE INFO

Keywords:
Zebrafish
Bone
Collagen
Imaging
Osteoblasts
Calcification

ABSTRACT

Type I collagen plays a pivotal role in shaping bone morphology and determining its physical properties by serving as a template for ossification. Nevertheless, the mechanisms underlying bone collagen formation, particularly the principles governing its orientation, remain unknown owing to the lack of a method that enables continuous in vivo observations. To address this challenge, we constructed a method to visualize bone collagen by tagging with green fluorescent protein (GFP) in zebrafish and observed the interactions between osteoblasts and collagen fibers during bone formation in vivo. When collagen type I alpha 2 chain (Col1a2)-GFP was expressed under the control of the osteoblast-specific promoters *osx* or *osc* in zebrafish, bone collagen was observed clearly enough to identify its localization, whereas collagen from other organs was not. Therefore, we determined that this method was of sufficient quality for the detailed in vivo observation of bone collagen. Next, bone collagen in the scales, fin rays, and opercular bones of zebrafish was observed in detail, when bone formation is more active. High-magnification imaging showed that Col1a2-GFP can visualize collagen sufficiently to analyze the collagen fiber orientation and microstructure of bones.

Furthermore, by simultaneously observation of bone collagen and osteoblasts, we successfully observed dynamic changes in the morphology and position of osteoblasts from the early stages of bone formation. It was also found that the localization pattern and orientation of bone collagen significantly differed depending on the choice of the expression promoter. Both promoters (*osx* and *osc*) used in this study are osteoblast-specific, but their Col1a2-GFP localizing regions within the bone were exclusive, with *osx* region localizing mainly to the outer edge of the bone and *osc* region localizing to the central area of the bone. This suggests the existence of distinct osteoblast subpopulations with different gene expression profiles, each of which may play a unique role in osteogenesis.

These findings would contribute to a better understanding of the mechanisms governing bone collagen formation by osteoblasts.

1. Introduction

Type I collagen secreted by osteoblasts aggregates to form a higher-order structure that serves as a scaffold (bone matrix) on which calcium-crystalline hydroxyapatite is deposited. Therefore, many of the physical properties of bone depend on the shape, orientation, and density of the collagen network (Georgiadis et al., 2016). Since collagen orientation can vary from a linear arrangement, in-plane crossing and layered overlapping, depending on the bone morphology and the direction of force application (Georgiadis et al., 2016; Reznikov et al., 2014), it is assumed that there is a precise control mechanism. Moreover, since abnormal collagen formation is responsible for pathological conditions such as osteogenesis imperfecta (OI) and various bone formation abnormalities (Marini et al., 2007), it is extremely important to elucidate its regulatory mechanisms.

To gain insight into the regulation of collagen formation and orientation during bone formation, it is essential to observe the dynamic behavior of collagen and the cells that secrete it in vivo. However, existing methods for observing collagen fibers do not fully satisfy this requirement. For example, they rely on fixed samples subjected to X-ray structural analysis, electron microscopy, and reagent staining of bone collagen (Reznikov et al., 2014). Some studies have also observed collagen in vivo by collagen-mimetic peptides (CMP) that bind specifically to collagen (Li et al., 2012; Yu et al., 2011) or by second harmonic generation (SHG) (Campagnola et al., 2002; Chen et al., 2012; LeBert et al., 2016; LeBert et al., 2015), but even using these methods, the localization of all collagen in real time is not directly reflected, and there are various limitations, such as the size and localization of the target

* Corresponding author.
E-mail address: jkuroda@fbs.osaka-u.ac.jp (J. Kuroda).

https://doi.org/10.1016/j.bonr.2024.101748
Received 13 November 2023; Received in revised form 21 February 2024; Accepted 3 March 2024
Available online 4 March 2024

collagen structure and detection sensitivity. Therefore, a new and novel method that allows in vivo observation of the process of collagen formation in the bone has been desired.

The most convenient way to visualize molecules in the body is to attach a fluorescent protein such as GFP to the target molecule. Therefore, many groups have labeled collagen 1 (Col1) molecules with GFP, however, it was difficult to clearly observe the fibrous structures. This is probably because the labeled Col1 molecules inhibit normal aggregation. However, recent efforts to devise binding positions have enabled the visualization of bone collagen in cultured osteoblasts and mouse skulls (Lu et al., 2018; Shiflett et al., 2019). In mice, there are physical limitations to observing whole-body bone collagen, however, more comprehensive observations are possible in more transparent animal species (Kashimoto et al., 2022; Morris et al., 2018). In this study, we developed transgenic zebrafish lines that expresses Col1a2-GFP in an osteoblast-specific manner and observed bone collagen in vivo during development. The simultaneous observation of collagen and osteoblasts provided insight into how osteoblasts form bone collagen.

2. Materials and methods

2.1. Zebrafish husbandry

We used the AB zebrafish strain to establish transgenic zebrafish lines. All fish were treated and used in the experiments in accordance with the guidelines and approved protocols for animal care and use at Osaka University, Japan. Zebrafish were maintained under standard laboratory conditions at 28.5 °C and a 14/10 h light/dark cycle.

2.2. Generation of zebrafish transgenic line

To create the *col1a2-gfp* sequence, we modified the zebrafish *col1a2* sequence by replacing the propeptide and telopeptide regions with *gfp* sequences, as previously described by Morris and colleagues (Morris et al., 2018). Initially, we generated pGEMT-*col1a2* by cloning the zebrafish *col1a2* sequence from a self-made zebrafish cDNA library into the pGEMT-easy vector using pGEM®-T Easy Vector Systems (Promega). Subsequently, a fragment containing the BamH1 insertion site, was created via mutagenic PCR. The *gfp* sequence was cloned and incorporated using NEBuilder HiFi DNA Assembly Master Mix (NEB). The *col1a2-gfp* sequence from the final pGEMT-*col1a2-gfp* construct was excised using restriction enzymes and inserted into the pTol2 vector, resulting in the generation of pTol2-*osteorix(osx):col1a2-gfp* and pTol2-*osteocalcin(osc):col1a2-gfp* constructs. The *osx* and *osc* promoter regions, known for their osteoblast-specific activity in medaka and also applicable to zebrafish (Inohaya et al., 2007; Renn and Winkler, 2009), were obtained from the genome using PCR. To prepare the osteoblast visualization transgenic line, we constructed pTol2–*3xosx:lifeact-yfp*, which incorporated the *lifeact-yfp* sequence into the pTol2 vector with three repeats of the *osx* promoter region using NEBuilder. Each plasmid was diluted with double-distilled water (DDW) to a final concentration of 50 ng/mL and injected into 1-cell stage embryos along with 25 ng/mL of transposase mRNA (Urasaki et al., 2006).

2.3. Confocal imaging and image processing

For imaging of whole fish body with a BZ- × 710 microscope (Keyence) equipped with a ×10 objective (NA 0.45 PlanApo), fish were anesthetized using tricaine (MS-222), placed on a glass dish.

For fixed fish bone sample imaging, euthanasia was performed using tricaine, followed by fixation in 4 % paraformaldehyde (PFA) in phosphate-buffered saline (PBS) at 4 °C overnight. Bone samples were imaged with a confocal microscope, Stellaris8 (Leica) with objectives HC PL APO 10×/0,40 CS2, HC PL APO 40×/1.30 OIL CS2, HC PL APO 63×/1,40 OIL CS2 (Leica) or LSM780 (Carl Zeiss) with objectives Plan-Apochromat 10×/0.45 M27 (Carl Zeiss), 20× NA 0.8 PlanApo (Carl Zeiss) and 63× NA 1.40 Oil PlanApo objective (Carl Zeiss). All images were analyzed using ZEN (Carl Zeiss), Imaris (Oxford Instruments) and LASX (Leica) to generate three-dimensional and sectional images.

2.4. Alizarin red staining

For Alizarin Red staining, live fish were immersed in a 0.005 % Alizarin Red solution at 28.5 °C overnight. Subsequently, the fish were returned to their tank water, and allowed to swim for 1 h for washing, and samples were collected.

2.5. Analysis of collagen fiber orientation

For analyzing collagen fiber orientation in scale, Fiji/ImageJ (NIH, USA) software was used. 20.0 μm square, and 3.67 μm thick (10slices) areas showing fiber structures clearly were extracted for analysis from z-stack images of Tg(*osx:col1a2-gfp*) fish scale using ZEN (Carl Zeiss). The orientation pattern of collagen fiber in each image was calculated as "Fourier components" with Directionality plugin (http://fiji.sc/wiki/index.php/Directionality). The slice images used for analysis were adjusted using the Fiji plugin, Enhance Local Contrast (Zuiderveld, 1994).

2.6. Temporal tracking of opercular bone growth

For analyzing the development of opercular bone from same Tg*(osx:col1a2-gfp)* fish at 7, 14 and 21 days post-fertilization (dpf) stained with Alizarin Red, the fish were anesthetized using tricaine (MS-222), placed on a glass dish and imaged with LSM780 (Carl Zeiss) with the objective of 20× NA 0.8 PlanApo (Carl Zeiss). The obtained images were analyzed with Imaris (Oxford Instruments).

2.7. Calculate bone mineral intensity

Tg(*osx:col1a2-gfp*) and its wild-type (WT) sibling fish at were scanned using micro–computed tomography (micro-CT) for calculation of bone mineral intensity. Four fish from each line were used for analysis. After overnight fixation with 4 % PFA, the samples were observed using micro-CT-scanner SkyScan 1172 (SkyScan NV, Aartselaar, Belgium) following the manufacturer's instructions. The X-ray source ranged from 35 kV, and the datasets were acquired at a resolution of 2.5 μm/pixel for whole body. The samples were scanned under air dry condition. After applying a fixed threshold for all samples, the average mineral intensity at five identical vertebrae segments were calculated with CT Analyzer (Bruker microCT).

3. Results

3.1. Expression of Col1a2-GFP in zebrafish osteoblasts enables systemic bone collagen visualization

Lu's group found a new insertion position that is not inhibitory to collagen molecules polymerization and can be visualized by GFP at telopeptide (Lu et al., 2018). We followed this method and bound GFP to the zebrafish *col1a2* gene. We also expressed *col1a2-gfp* under the control of the osteoblast marker gene *osterix*-derived promoter (Renn and Winkler, 2009) to specifically visualize bone collagen (See Fig. 1A for construct details). A whole-body image of the Tg(*osx:col1a2-gfp*) larvae at 14 days post fertilization (dpf) obtained by gene transfer is shown in Fig. 1. The GFP signal was consistent with the location of Alizarin Red-labeled bone, suggesting Col1a2-GFP localization in the bone (Fig. 1B, C and D). The background fluorescence was also very low, indicating that collagen other than bone was not labeled by Col1a2-GFP. To examine whether bone calcification is proper in our Tg fish, we analyzed the mineral intensity of Tg(*osx:col1a2-gfp*) fish using micro-CT and compared them with their WT siblings (Sup. Fig. 1). As a result, there

was no significant difference between bone mineral intensity of Tg and WT. This indicated that the expression of Col1a2-GFP during bone formation didn't perturb the normal calcification of bones. Because bone collagen-specific labeling was obtained as expected, we next used this line to examine the later stages of osteogenesis in more detail.

3.2. Bone collagen fibers visualized by Col1a2-GFP exhibit normal orientation pattern

Scales, which correspond to the dermal bone, are a valuable resource for bone research owing to their location on the surface of the fish body, which makes them easily observable and amputable (Sire and Akimenko, 2004; Sire et al., 1997). Given that previous studies have reported the detection of *osx* expression in scales and that electron microscopy observations have revealed a well-ordered, collagen-based layered structure within these scales(Iwasaki et al., 2018; Kobayashi-Sun et al., 2020), we initiated our investigation by examining the localization of Col1a2-GFP in scales. Fig. 2A shows a whole-body image of a 2-month-old zebrafish, clearly showing the outline of the scales. When the scales were peeled off and observed directly with a confocal microscope (Fig. 2B), a concentric circular pattern was visible. The fluorescence of GFP was stronger at the center of the scales and weaker at the edges. 3D view of the scale revealed a Col1a2-GFP accumulation layer separated from the Alizarin Red stained layer (Fig. 2C). In the previous studies, it was reported that there are 3 type layers in scales. The limiting layer and external layer, localizing on the body surface side of scales, are calcified and stained well with Alizarin Red (Sire and Akimenko, 2004). On the other hand, elasmoid layer composed of many thin layers exhibits low or no calcification (Sire and Akimenko, 2004). Therefore, it was suggested that this Col1a2-GFP accumulation at the scales localized to the elasmoid layers. When the area with strong GFP fluorescence was observed at higher magnification, the collagen structure could be detected as aligned fibers in one or two uniform direction (s) (Fig. 2D, F, Sup. Fig. 2). After successfully detecting collagen in the scales as fibers, we next attempted to analyze the orientation of the collagen fibers in the scales. To analyze collagen fiber orientation in detail, we first chose the area of 20 μm square and 3.67 μm thick (total of 10 xy slice images along the axis from surface to deep), as shown in Fig. 2 B and C, and then observed collagen fibers in each slice. The orientation of the collagen fibers in each slice gradually changed along the surface in deeper direction (Fig. 2D, F, Sup. Fig. 2). As a result of the calculation of fiber orientation at each slice, we found that the orientation pattern of fibers in the elasmoid layer was classified into two characteristic slices group, 'lattice-like' slice and 'border-like' slice (Fig. 2D-G, Sup. Fig. 2). In the lattice-like slice, the angle distribution showed a fiber orientation concentrated in two directions (Fig. 2D, E, Sup. Fig. 2). On the other hand, in the border-like slice, the angle distribution showed a fiber orientation concentrated in one direction (Fig. 2F, G, Sup. Fig. 2). The orientation pattern of collagen fibers in the elasmoid layer of Tg fish was similar to that reported in previous studies (Campagnola et al., 2002; Feng et al., 2020; Zylberberg et al., 1988). This suggests that Col1a2-GFP can assemble with endogenous collagen molecules to visualize the normal network of collagen fibers in Tg bones.

3.3. Localization of bone collagen visualized by Col1a2-GFP varies depending on the promoter

As shown in Fig. 2B, the GFP signal was stronger in the center and weaker at the margins in the scale (Fig. 2B). Furthermore, it was localized under osteoblasts and not in calcified area stained with Alizarin Red (Fig. 2C). We considered the possibility that this region specificity might depend on the nature of the *osx* promoter and decided to create a Col1a2-GFP construct using a promoter derived from osteocalcin (*osc*), another osteoblast-specific marker gene, to compare their Col1a2-GFP localizing regions. It is known that *osteocalcin* expression is weak in the scales, and indeed, fluorescence signal of Col1a2-GFP could not be confirmed in the scales of Tg(*osc:col1a2-gfp*) fish. However, Col1a2-GFP in the *osc* promoter line was observed in the fin ray and opercular bones, both of them are often used for bone research in zebrafish because of their ease of observation (Hammond and Moro, 2012; Kimmel et al., 2010). However, the Col1a2-GFP distribution in Tg(*osc:col1a2-gfp*) bones was different from that in the Tg*(osx:col1a2-gfp)* bones (Figs. 3 and 4).

As shown in Fig. 3A and B, under the *osx* promoter, Col1a2-GFP localized near the articular regions of the fin ray bone. In contrast, under the control of the *osc* promoter, it was predominantly observed in

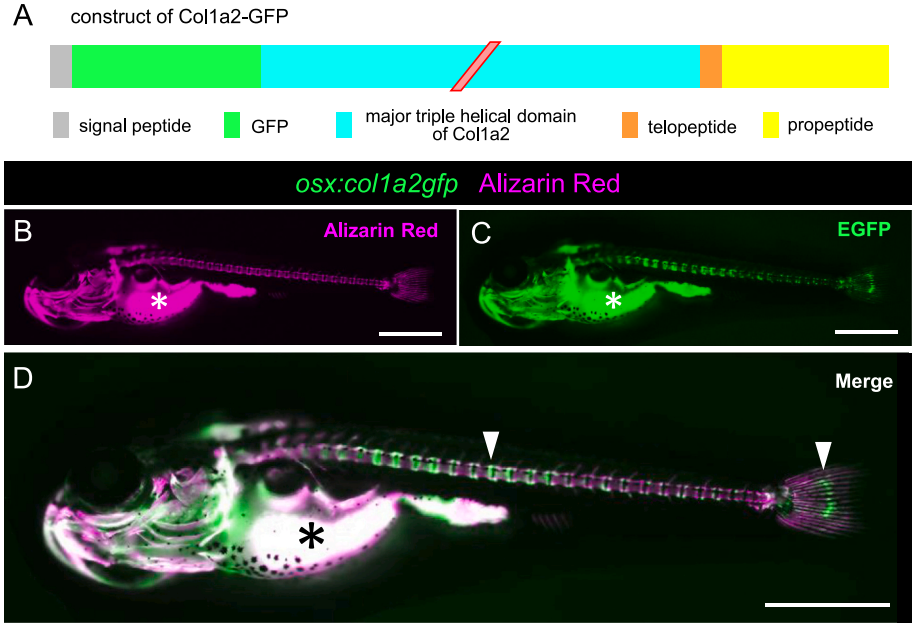

Fig. 1. Col1a2-GFP distribution pattern in Tg(*osx:col1a2-gfp*) fish at 14 days post fertilization (dpf) with Alizarin Red staining.
(A) A schematic illustration of the expression construct of col1a2-gfp.
(B, C, D) Alizarin Red signal (B), GFP signal (C), Merged (D) image of Tg(*osx:col1a2-gfp*) fish with Alizarin Red staining. * in A, B and C show auto-fluorescence in the yolk. Strong accumulations of Col1a2-GFP were observed at specific sites of bones (arrowheads). Scale bar = 1 mm.

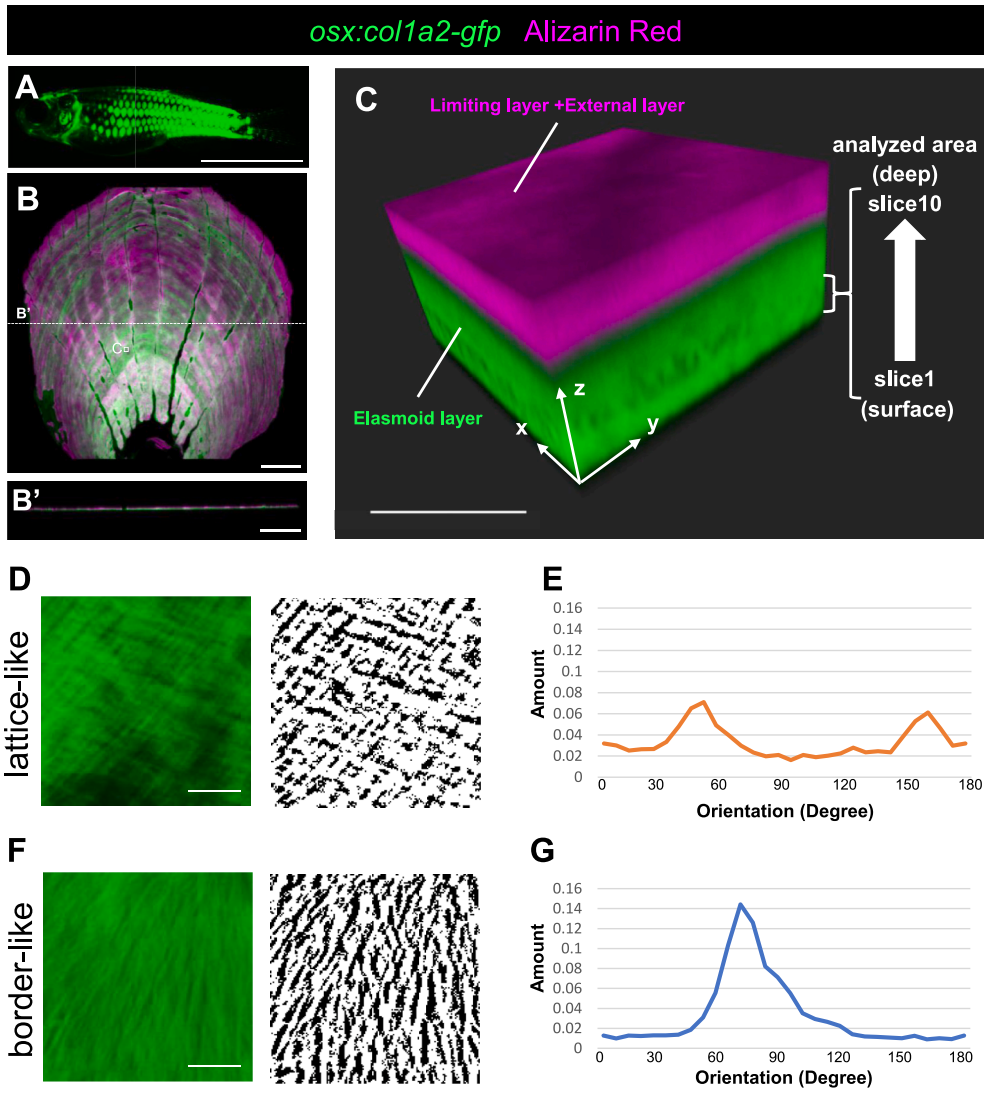

Fig. 2. Fluorescent images of the scales from Tg(*osx:col1a2-gfp*) fish.
(A) GFP signal of the whole body in Tg(*osx:col1a2-gfp*) 2 months-old-fish. Scales are visualized by GFP fluorescence. Scale bar = 5 mm.
(B) Whole image of single scale isolated from Tg(*osx:col1a2-gfp*) fish stained with Alizarin Red. (B′) indicates section view at dot line B′ in B. Scale bar = 200 μm.
(C) 3D view of the high magnification image at box C (20 μm square) in (B). The limiting and external layers are well-calcified, as shown by Alizarin Red staining. The elasmoid layer has low or no calcification with abundant Col1a2-GFP. ten z-stack slice images (each slice has 0.367 μm thickness) at elasmoid layer were selected as analyzed area (10 slices, total 3.67 μm depth) for analysis of collagen fiber orientation (D, E, F, G and Sup. Fig. 2). White arrow with surface and deep indicates surface-deep axis in the analyzed area. Scale bar = 10 μm.
(D) Left image shows a slice view of lattice-like collagen fibers in the analyzed area at C. Right image shows an adaptive thresholding view to enhance the fiber edges of the left image. Scale bar = 5 μm.
(E) Orientation histogram of collagen fiber shown in D.
(F) Left image shows a slice view of border-like collagen fibers in the analyzed area at C. Right image shows an adaptive thresholding view to enhance the fiber edges of the left image. Scale bar = 5 μm.
(G) Orientation histogram of the collagen fiber shown in F.

the central part of the fin ray bone (Fig. 3C, D). With the *osx* promoter, collagen fibers tended to align along the long-axis direction of the fin ray bone (Fig. 3B), whereas no distinct orientation was observed with the *osc* promoter (Fig. 3D). Moreover, the localization pattern in the cross-section also exhibited clear differences: under the *osx* promoter, GFP localization was confined to the inside of the fin ray bone (as Alizarine Red stains only the surface of the fin ray bone), whereas under the *osc* promoter, Col1a2-GFP was primarily found on the inner surface of the curved fin ray bone (Fig. 3B′, B″, D′, D″).

In the opercular bone, Col1a2-GFP localization expressed under the two promoters also showed partially overlapping but roughly exclusive patterns. Under the *osx* promoter, strong GFP signals were localized in the proximal region and near the outer edge of the fan-shaped opercular bone (Fig. 4A). In contrast, under the *osc* promoter, Col1a2-GFP was localized around the central region of the fan (Fig. 4B). In addition, the overall GFP pattern tended to be arranged in an arc-like pattern (Fig. 4A, A" arrowhead). This arc-like localization is consistent with the progressive zones of annual growth observed in the growth analysis of opercular bones using Alizarin Red staining (Kimmel et al., 2010). Similar arcuate striations were observed in the opercular bone of the Tg (*osc:col1a2-gfp*) fish, but the Col1a2-GFP localizing area differed from that of Tg(*osx:col1a2-gfp*) fish because they were more extensive (Fig. 4B, B").

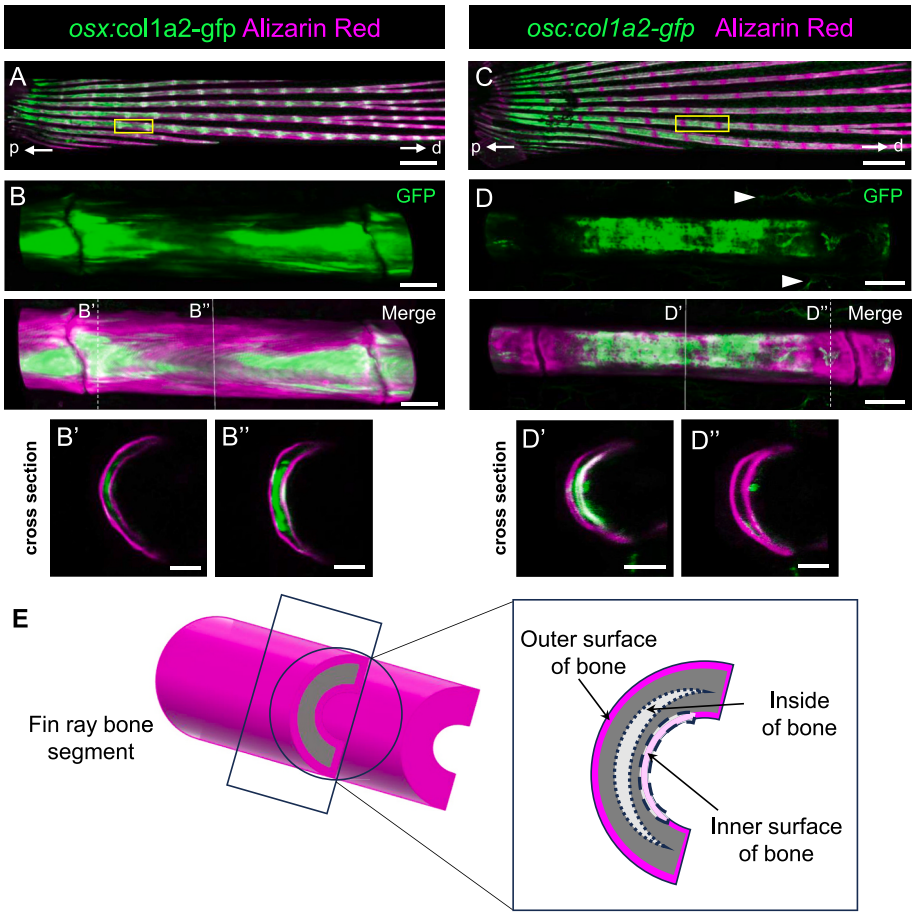

Fig. 3. Fluorescent images of fin ray bones from Tg(*osx:col1a2-gfp*) and Tg(*osc:col1a2-gfp*) fish.
(A, C) Fin ray bones stained with Alizarin Red in Tg(*osx:col1a2-gfp*) (A) and Tg(*osc:col1a2-gfp*) (C). Arrows p, d indicate proximal-distal axis of fin ray bones.
(B, D) Magnified image of yellow box in (A, C). Arrowheads in (D) indicate autofluorescence of blood vessels.
(B′, B″ and D′, D″) Section views at lines B′, B″ and lines D′, D″ in B, D.
(E) Illustration of fin ray bone segment. Col1a2-GFP driven by *osx* promoter was detected on the inner side of the bone at the edge of bone segment (B″) but detected weakly at middle of the bone segment (B′). Driven by *osc* promotor, it was detected at inner surface of bone at middle of bone segment (D′) but was detected significant weakly detectedat the edge of the bone segment (D″). Scale bar = 400 μm (A, C), 40 μm (B, D) and 20 μm (B′, B″, D′, D″).

3.4. Simultaneous observation of bone collagen and osteoblasts facilitates osteoblast dynamics analysis during bone collagen formation

The opercular bone is one of the first to form during development and is located near the body surface, making it a suitable model for observing bone formation. To gain insight into osteoblast dynamics and their role in bone collagen formation, we crossed the osteoblast visualization line Tg(*3xosx:lifeact-yfp*) with Tg(*osx:col1a2-gfp*) and observed the growth of the opercular bone during the early stages of development (3, 5 and 7 dpf) (Fig. 5).

In embryos at 3 dpf, the formation of oval pouch-like osteoblast populations was observed, and collagen structures were found in the space inside these pouch-like populations of oval osteoblasts (Fig. 5A, B, C). At 5 dpf, the collagen structures extended along the proximal-distal axis and were surrounded by cell populations. By 7 dpf, the opercular bone had a characteristic fan-shaped morphology (Fig. 5D, E, F, G, H, I, J). During this period, the cells surrounding the collagen structure gradually shifted from an almost spherical morphology to a flattened one (Fig. 5C′, C″, F″, F″, J", J"). Furthermore, strong YFP fluorescence was consistently observed throughout all developmental stages at sites where the cells were in contact with the collagen structures (Fig. 5C, F, J). In Tg(*3xosx:lifeact-yfp*) fish, lifeact-YFP expressed in osteoblasts visualizes their actin fibers (Riedl et al., 2008). Thus, prominent YFP fluorescence at the cell-collagen interface indicated actin-rich regions. Furthermore, alizarin red staining revealed that calcification occurred within the bone collagen at 7 dpf (Fig. 5G, H, I, J).

3.5. Temporal tracking of bone collagen and its calcification

The method developed in this study, visualizing collagen fibers in zebrafish bone by Col1a2-GFP, enables temporal observation of the subjects without killing and fixing them. To analyze the growth and calcification of the bone, we repeatedly stained the opercular bone of the same individual Tg(*osx:col1a2-gfp*) fish with Alizarin Red for each imaging at 7, 14 and 21 dpf, and observed the changes between each stage (Fig. 6). We confirmed that the bone collagen structure indicated by Col1a2-GFP extended anisotropically as it grew, and the calcified areas indicated by the Alizarin Red signal expanded within the bone collagen following its growth (Fig. 6A, B). We analyzed the Alizarin Red-positive areas within the regions showing the Col1a2-GFP signal and found that in the peripheral area of the opercular bone, there were two types of areas: one where mineralization had progressed to the end, and another where only Col1a2-GFP was detected without any Alizarin Red signal (Fig. 6B). Such uncalcified areas, where only Col1a2-GFP was localized were well-aligned with the direction in which the opercular bone would later extend (Fig. 6B, arrow).

4. Discussion

In this study, by expressing Col1a2-GFP in zebrafish under the

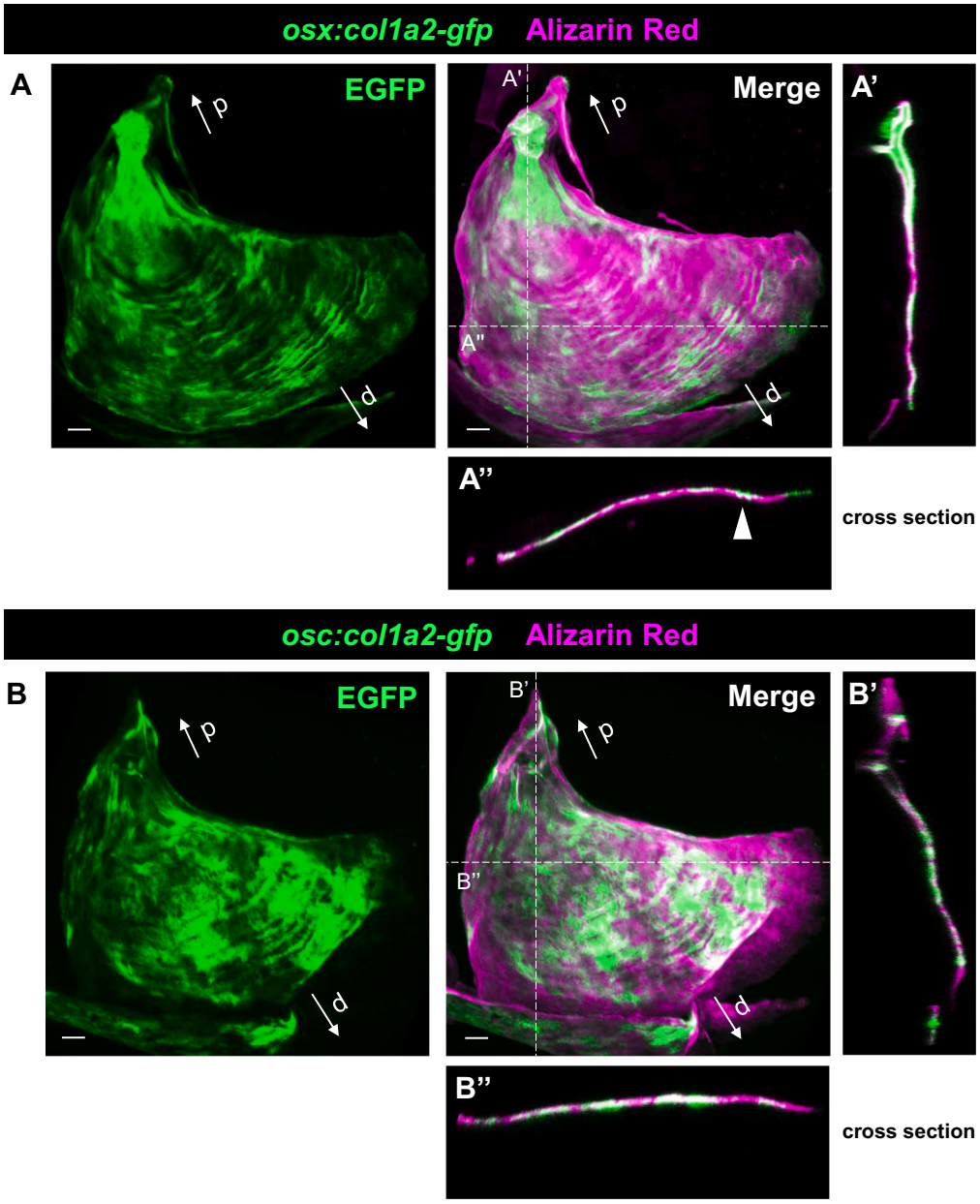

Fig. 4. Fluorescent images of the opercular bones from Tg(*osx:col1a2-gfp*) and Tg(*osc:col1a2-gfp*) fish.
(A, B) The opercular bones stained with Alizarin Red isolated from Tg(*osx:col1a2-gfp*) (A) and Tg(*osc:col1a2-gfp*) (B) fish. Arrows p, d indicate the proximal-distal axis of opercular bones.
(A′, A″) Cross-sectional images at white dotted lines A′, A″ in A.
(B′, B″) Cross-sectional images at white dotted lines B′, B″ in B. Arrowhead in (A″) indicates a strong accumulation of Col1a2-GFP at limited sites. Scale bar = 20 μm.

control of two osteoblast-specific promoters, we succeeded in visualizing collagen in bones such as fin ray, opercular bones and scales specifically and clearly enough to reveal the orientation of the fibers. We also succeeded in simultaneously observing osteogenesis (calcification), collagen, and osteoblasts responsible for collagen synthesis in three dimensions (Figs. 5, 6). These results demonstrate that the techniques used in this study serve as valuable tools for investigating the complexities of collagen dynamics and osteogenic processes, yielding several noteworthy findings, as detailed below.

In this study, it was shown that in the scales of Tg(o*sx:col1a2-gfp*) fish, Col1a2-GFP specifically accumulated in the elasmoid layer (Fig. 2B, C). These Col1a2-GFP signals in the scales were strong enough to detect and analyze fiber orientation in detail (Fig. 2C, D, F, Sup. Fig. 2). As a result of the fiber orientation analysis, we found two characteristic slice groups, namely, border-like slices and lattice-like slices (Fig. 2E, G, Sup. Fig. 2). Interestingly, these two slice groups were arranged sequentially along the axis from the surface to the deeper parts of the scale (Sup. Fig. 2). Previous studies have reported that the elasmoid layer is composed of thin layers of collagen stacked together, and the collagen fibers within each thin layer are aligned in a specific orientation and the orientation shifts with each successive layer, thereby forming a bouligand structure (Feng et al., 2020; Sire and Akimenko, 2004; Zylberberg et al., 1988). It is suggested that the unique orientation of collagen in the two types slice groups can be attributed to the positioning of the border-like slices within a single thin layer of the elasmoid layer, and the lattice-like slices at the transition area between the two thin layers. These results suggested that Col1a2-GFP could accurately replicate the endogenous collagen structure within the scales in detail. Therefore, we

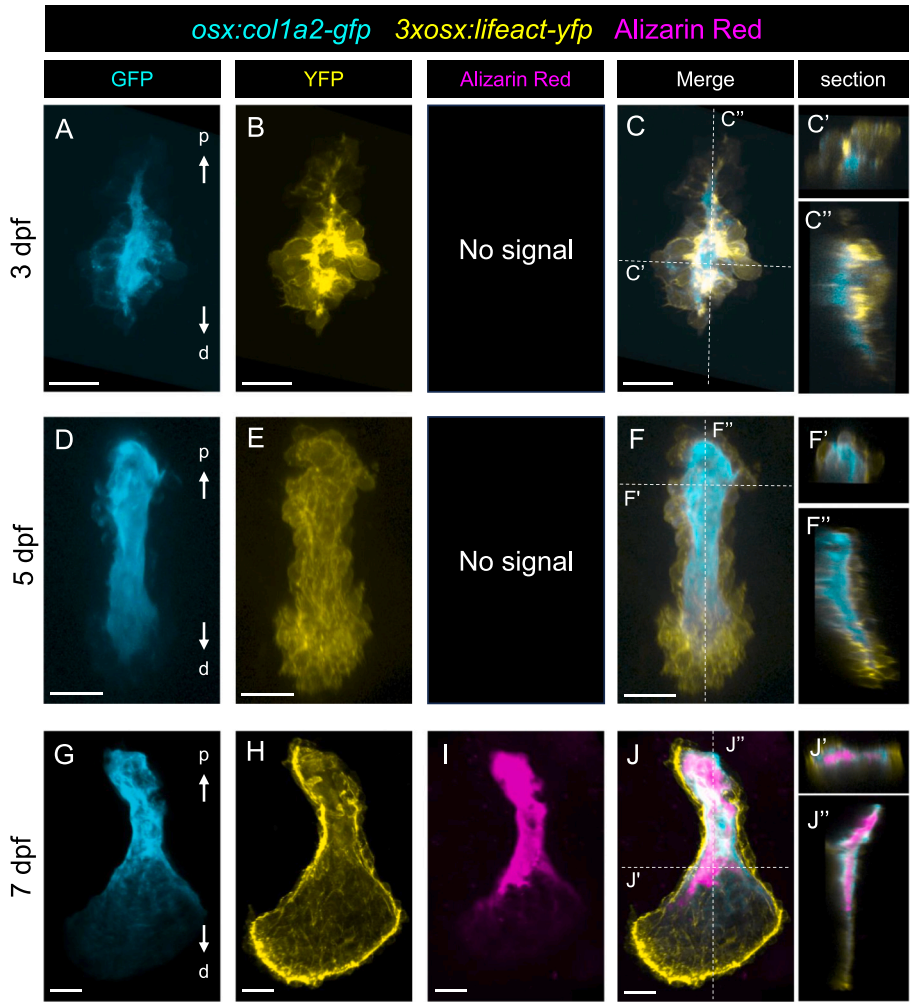

Fig. 5. Developmental process of the opercular bone in Tg(*osx:col1a2-gfp; 3xosx:lifeact-yfp*) fish at early stages.
(A, D, G) Collagen structures of the opercular bone from different larvae at 3 dpf (A), 5 dpf (D) and 7 dpf (G). Arrows p, d indicate proximal-distal axis.
(B, E, H) Osteoblasts forming opercular bone at 3 dpf (B), 5 dpf (E) and 7 dpf (H).
(I) Alizarin Red signal in the opercular bone. This signal was detected in only 7 dpf larvae. (C, F, J) Merged view of (A, B), (D, E) and (G, H, I).
(C′, C″, F′, F″, J′, J″) Cross-sectional views at white dotted line C′, C″, F′, F″, J′, J″ in (C), (F) and (J). Scale bar = 20 μm.

concluded that the observation method for bone collagen using Col1a2-GFP described in this study can be used to analyze the orientation pattern of bone collagen fibers, which is important for the mechanical properties of bones. In the future, by developing strains with a wide range of Col1a2-GFP expression in bones and improving the observation methods, it is expected that a more detailed analysis of collagen microstructure in vivo can be performed.

In this study, we used two transgenic lines, Tg(*osx:col1a2-gfp*) and Tg (*osx:col1a2-gfp*). Both *osx* and *osc* are known osteoblast-specific marker genes (Inohaya et al., 2007; Renn and Winkler, 2009), but Tg(*osx:col1a2-gfp*) and Tg(*osx:col1a2-gfp*) showed different localization of Col1a2-GFP in bones from each other. These different localizations of Col1a2-GFP expressed under *osx* and *osc* promotors suggested that osteoblast populations may have subpopulations with different gene expression, as reported in scales (Iwasaki et al., 2018). *osx* functions in the differentiation of osteoblasts and is expressed from the middle to the end of the differentiation period, as reported in previous studies (Nakashima et al., 2002; Sun et al., 2008; Zou et al., 2006). On the other hand, it is reported that *osc* is expressed in mature osteoblasts and plays a role in bone calcification and homeostasis maintenance (Berezovska et al., 2019; Ducy et al., 1996; Komori, 2015). From these findings, it is expected that the subpopulation of immature osteoblasts expressing *osx* is localized in growing areas, and the subpopulation of mature osteoblasts expressing *osc* is localized in areas where calcification occurs in the bone. In fact, Col1a2-GFP under the *osx* promoter strongly accumulated in the growing areas of the opercular bone and distal edge (Figs. 4, 6) (Kimmel et al., 2010), and Col1a2-GFP under the *osc* promoter mainly accumulated in the calcified areas indicated by Alizarin Red signals (Figs. 3, 4). These data suggested that subpopulations of osteoblasts with different gene expression patterns may be localized in different parts of the bone and that each population may be responsible for the formation of different parts of the bone that show different collagen microstructure patterns (Georgiadis et al., 2016; Iwasaki et al., 2018; Ofer et al., 2019). For further verification of this hypothesis, it is necessary to perform gene expression analysis on osteoblast populations and confirm whether subpopulations show different gene expression and localization other than those expressing *osx* and *osc*.

We also successfully observed morphological changes and calcification of opercular bone during early (3, 5, 7 dpf) development. The collagen matrix initially started to be formed in a pouch like clusters of rounded osteoblasts and then changed into a characteristic fan-like shape (Fig. 5). Simultaneously, the shapes of the surrounding osteoblasts also gradually changed from spherical to flat (Fig. 5C', C", F", F"', J", J"), similar to the observation results in previous studies (Huycke et al., 2012; Kimmel et al., 2010). The initial round shape of osteoblasts may be due to the absence of an extracellular matrix (collagen) to serve

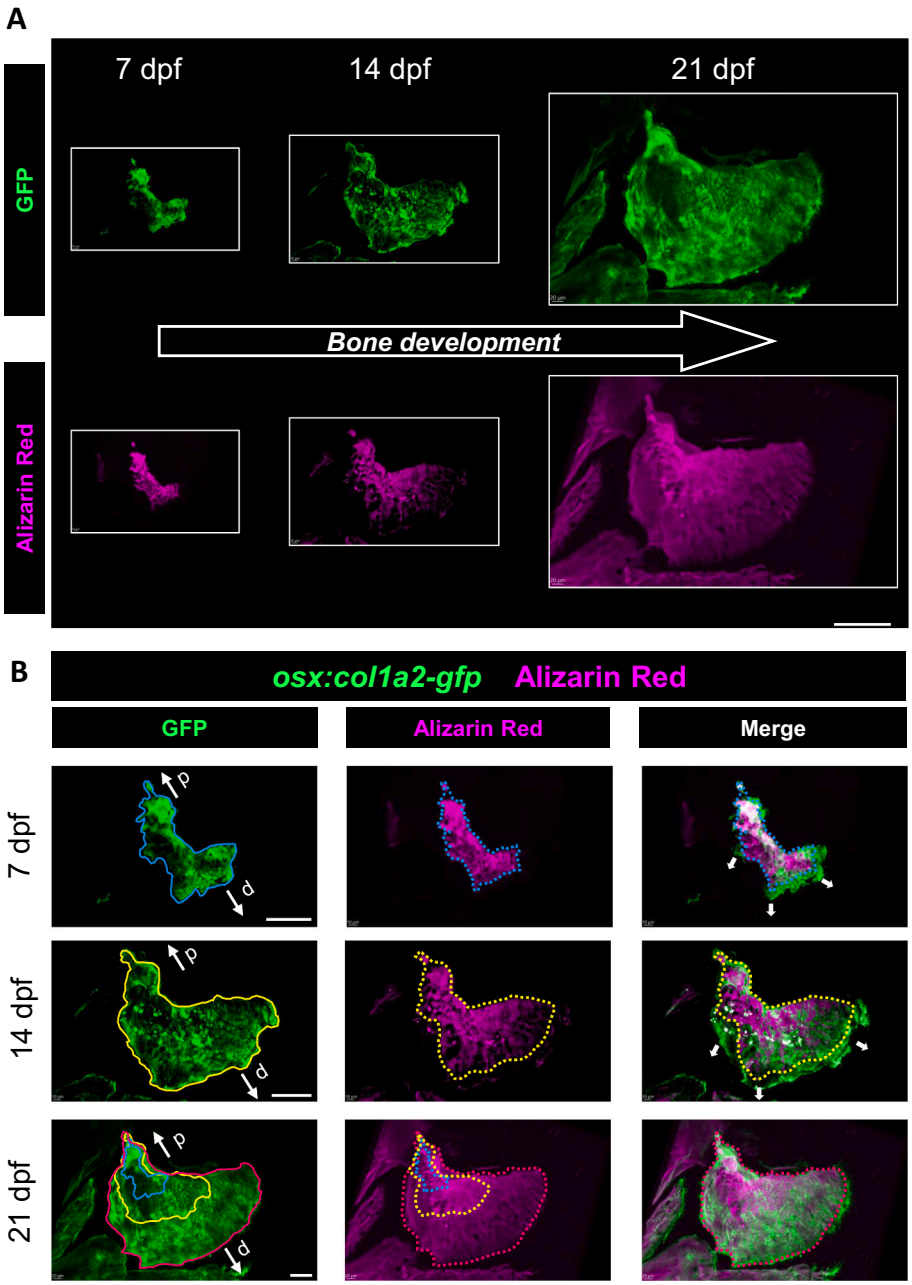

Fig. 6. Growing and calcification analysis of opercular bone.
(A) Same scale views of the opercular bones stained with Alizarin Red in the same living Tg(*osx:col1a2-gfp*) fish at 7, 14 and 21 dpf. Right-side views with dorsal approximately to the top and anterior to the left. Scale bar = 100 μm.
(B) 3D images of the opercular bones at 7, 14 and 21 dpf in (A). The blue, yellow and magenta lines show Col1a2-GFP shapes at 7, 14 and 21 dpf. The blue, yellow and magenta dotted lines show the bone shapes indicated by Alizarin Red at 7, 14 and 21 dpf. White arrows indicate Col1a2-GFP accumulation without Alizarin Red signals. Arrows p, d indicate proximal-distal axis. Scale bar = 50 μm.

as a scaffold. In the previous studies, it was also reported that altered extracellular matrix structures cause morphological changes in the osteoblasts in other bones and in vitro culture assays (Kimmel et al., 2010; Matsugaki et al., 2015; Shiflett et al., 2019; Tsai et al., 2022).

Our method using the Col1a2-GFP expression system allows us to observe bone collagen in living fish. With this strong advantage, we succeeded in observing the time-series development of the opercular bone. By temporal observation of the developing opercular bone in the same fish, we tracked the bone collagen dynamics during development with calcification. the opercular bone at 7, 14 and 21 dpf fish showed anisotropic growth (Fig. 6), consistent with the results of previous study (Kimmel et al., 2010). The previous study reported that opercular bone shows low elongation at the proximal edge and high elongation at the distal edge. At the distal edge, which has been reported as a well-growing site, Col1a2-GFP accumulation without Alizarin Red staining was observed (Fig. 6A). This indicates that Col1a2-GFP secretion actively occurs at the growth site of the opercular bone from Tg(*osx:col1a2-gfp*) fish, where high *osx* expression has been reported (Kimmel et al., 2010). Because calcification occurs after bone collagen accumulation, the dominant secretion of Col1a2-GFP at the growth site may form a GFP-positive area that is not yet calcified.

Osteoblasts perform not only bone collagen secretion but also bone calcification induced by the secretion of hydroxyapatite. In the observations of this study, calcification in the opercular bone at early stage of

development proceeded from within the collagen structure rather than from the surface, where it was in contact with osteoblasts (Fig. 5I, J, J', J"). This pattern of calcification was also observed in the regenerating fin ray bone, with calcification progressing from the inside of the bone (Sup. Fig. 3). Calcification from areas not in contact with osteoblasts suggested that osteoblasts may extend their cellular projections into the collagen and secrete hydroxyapatite from within the collagen structure. In fact, in regenerating fin rays, numerous holes were observed in the bone collagen surrounding the calcification sites (Sup. Fig. 3, white arrows), suggesting that the cellular protrusions of osteoblasts extend to the inside of the regenerating fin ray bones through these holes and promote calcification from there. More detailed observations of the osteoblast dynamics during bone formation may allow us to answer this question.

A abnormal orientation of bone collagen fibers and calcification in bones are typical symptoms of OI (Marini et al., 2007). Regarding OI research, multiple OI model strains have been reported in zebrafish and used for analyzing their symptoms and treatments (Huang et al., 2021; Marí-Beffa et al., 2021). In this study, it was demonstrated that collagen orientation and calcification can be observed in vivo through Col1a2-GFP expression in bone. Our new technique for visualizing bone collagen enables us to closely observe the dynamics of collagen structure and the progression of calcification in living zebrafish. Therefore, it provides a valuable tool for analyzing the phenotype of OI model fish and exploring the impact of candidate molecules for therapeutic drugs on these aspects.

Supplementary data to this article can be found online at https://doi.org/10.1016/j.bonr.2024.101748.

CRediT authorship contribution statement

Hiromu Hino: Writing – original draft, Visualization, Investigation. **Shigeru Kondo:** Writing – review & editing, Supervision, Project administration, Funding acquisition, Conceptualization. **Junpei Kuroda:** Project administration.

Declaration of competing interest

The authors declare that they have no known competing financial interests or personal relationships that could have appeared to influence the work reported in this paper.

Data availability

Data will be made available on request.

Acknowledgements

We thank the members of the Kondo laboratory for their experimental support and comments on this work. This work was supported by FBS Core Facility at Osaka University. We thank FBS Core Facility at Osaka University for technical support.

Confocal images were acquired (with LSM780) at FBS Core Facility and (With Stellaris8 (Leica)) at Leica imaging lab at Osaka University. This work was supported by JSPS KAKENHI, Grant Number 20H05943, JSPS KAKENHI, Grant Number 21H00327, JST FOREST Program, Grant Number JPMJFR224P, Japan.

References

Berezovska, O., Yildirim, G., Budell, W.C., Yagerman, S., Pidhaynyy, B., Bastien, C., Dowd, T.L., 2019. Osteocalcin affects bone mineral and mechanical properties in female mice. Bone 128, 115031. https://doi.org/10.1016/j.bone.2019.08.004.

Campagnola, P.J., Millard, A.C., Terasaki, M., Hoppe, P.E., Malone, C.J., Mohler, W.A., 2002. Three-dimensional high-resolution second-harmonic generation imaging of endogenous structural proteins in biological tissues. Biophys. J. 82 (1 Pt 1), 493–508. https://doi.org/10.1016/S0006-3495(02)75414-3.

Chen, X., Nadiarynkh, O., Plotnikov, S., Campagnola, P.J., 2012. Second harmonic generation microscopy for quantitative analysis of collagen fibrillar structure. Nat. Protoc. 7 (4), 654–669. https://doi.org/10.1038/nprot.2012.009.

Ducy, P., Desbois, C., Boyce, B., Pinero, G., Story, B., Dunstan, C., Karsenty, G., 1996. Increased bone formation in osteocalcin-deficient mice. Nature 382 (6590), 448–452. https://doi.org/10.1038/382448a0.

Feng, H., Li, X., Deng, X., Guo, J., Ma, K., Jiang, B., 2020. The lamellar structure and biomimetic properties of a fish scale matrix. RSC Adv. 10 (2), 875–885. https://doi.org/10.1039/c9ra08189e.

Georgiadis, M., Müller, R., Schneider, P., 2016. Techniques to assess bone ultrastructure organization: orientation and arrangement of mineralized collagen fibrils. J. R. Soc. Interface 13 (119). https://doi.org/10.1098/rsif.2016.0088.

Hammond, C.L., Moro, E., 2012. Using transgenic reporters to visualize bone and cartilage signaling during development in vivo. Front Endocrinol (Lausanne) 3, 91. https://doi.org/10.3389/fendo.2012.00091.

Huang, H., Liu, J., Zhang, G., 2021. A novel de novo mutation in COL1A1 leading to osteogenesis imperfecta confirmed by zebrafish model. Clin. Chim. Acta 517, 133–138. https://doi.org/10.1016/j.cca.2021.02.024.

Huycke, T.R., Eames, B.F., Kimmel, C.B., 2012. Hedgehog-dependent proliferation drives modular growth during morphogenesis of a dermal bone. Development 139 (13), 2371–2380. https://doi.org/10.1242/dev.079806.

Inohaya, K., Takano, Y., Kudo, A., 2007. The teleost intervertebral region acts as a growth center of the centrum: in vivo visualization of osteoblasts and their progenitors in transgenic fish. Dev. Dyn. 236 (11), 3031–3046. https://doi.org/10.1002/dvdy.21329.

Iwasaki, M., Kuroda, J., Kawakami, K., Wada, H., 2018. Epidermal regulation of bone morphogenesis through the development and regeneration of osteoblasts in the zebrafish scale. Dev. Biol. 437 (2), 105–119. https://doi.org/10.1016/j.ydbio.2018.03.005.

Kashimoto, R., Furukawa, S., Yamamoto, S., Kamei, Y., Sakamoto, J., Nonaka, S., Satoh, A., 2022. Lattice-patterned collagen fibers and their dynamics in axolotl skin regeneration. iScience 25 (7), 104524. https://doi.org/10.1016/j.isci.2022.104524.

Kimmel, C.B., DeLaurier, A., Ullmann, B., Dowd, J., McFadden, M., 2010. Modes of developmental outgrowth and shaping of a craniofacial bone in zebrafish. PLoS One 5 (3), e9475. https://doi.org/10.1371/journal.pone.0009475.

Kobayashi-Sun, J., Yamamori, S., Kondo, M., Kuroda, J., Ikegame, M., Suzuki, N., Kobayashi, I., 2020. Uptake of osteoblast-derived extracellular vesicles promotes the differentiation of osteoclasts in the zebrafish scale. Commun Biol 3 (1), 190. https://doi.org/10.1038/s42003-020-0925-1.

Komori, T., 2015. Animal models for osteoporosis. Eur. J. Pharmacol. 759, 287–294. https://doi.org/10.1016/j.ejphar.2015.03.028.

LeBert, D.C., Squirrell, J.M., Rindy, J., Broadbridge, E., Lui, Y., Zakrzewska, A., Huttenlocher, A., 2015. Matrix metalloproteinase 9 modulates collagen matrices and wound repair. Development 142 (12), 2136–2146. https://doi.org/10.1242/dev.121160.

LeBert, D.C., Squirrell, J.M., Huttenlocher, A., Eliceiri, K.W., 2016. Second harmonic generation microscopy in zebrafish. Methods Cell Biol. 133, 55–68. https://doi.org/10.1016/bs.mcb.2016.01.005.

Li, Y., Foss, C.A., Summerfield, D.D., Doyle, J.J., Torok, C.M., Dietz, H.C., Yu, S.M., 2012. Targeting collagen strands by photo-triggered triple-helix hybridization. Proc. Natl. Acad. Sci. USA 109 (37), 14767–14772. https://doi.org/10.1073/pnas.1209721109.

Lu, Y., Kamel-El Sayed, S.A., Wang, K., Tiede-Lewis, L.M., Grillo, M.A., Veno, P.A., Dallas, S.L., 2018. Live imaging of type I collagen assembly dynamics in osteoblasts stably expressing GFP and mCherry-tagged collagen constructs. J. Bone Miner. Res. 33 (6), 1166–1182. https://doi.org/10.1002/jbmr.3409.

Marí-Beffa, M., Mesa-Román, A.B., Duran, I., 2021. Zebrafish models for human skeletal disorders. Front. Genet. 12, 675331 https://doi.org/10.3389/fgene.2021.675331.

Marini, J.C., Forlino, A., Cabral, W.A., Barnes, A.M., San Antonio, J.D., Milgrom, S., Byers, P.H., 2007. Consortium for osteogenesis imperfecta mutations in the helical domain of type I collagen: regions rich in lethal mutations align with collagen binding sites for integrins and proteoglycans. Hum. Mutat. 28 (3), 209–221. https://doi.org/10.1002/humu.20429.

Matsugaki, A., Isobe, Y., Saku, T., Nakano, T., 2015. Quantitative regulation of bone-mimetic, oriented collagen/apatite matrix structure depends on the degree of osteoblast alignment on oriented collagen substrates. J. Biomed. Mater. Res. A 103 (2), 489–499. https://doi.org/10.1002/jbm.a.35189.

Morris, J.L., Cross, S.J., Lu, Y., Kadler, K.E., Dallas, S.L., Martin, P., 2018. Live imaging of collagen deposition during skin development and repair in a collagen I - GFP fusion transgenic zebrafish line. Dev. Biol. 441 (1), 4–11. https://doi.org/10.1016/j.ydbio.2018.06.001.

Nakashima, K., Zhou, X., Kunkel, G., Zhang, Z., Deng, J.M., Behringer, R.R., de Crombrugghe, B., 2002. The novel zinc finger-containing transcription factor osterix is required for osteoblast differentiation and bone formation. Cell 108 (1), 17–29. https://doi.org/10.1016/s0092-8674(01)00622-5.

Ofer, L., Dumont, M., Rack, A., Zaslansky, P., Shahar, R., 2019. New insights into the process of osteogenesis of anosteocytic bone. Bone 125, 61–73. https://doi.org/10.1016/j.bone.2019.05.013.

Renn, J., Winkler, C., 2009. Osterix-mCherry transgenic medaka for in vivo imaging of bone formation. Dev. Dyn. 238 (1), 241–248. https://doi.org/10.1002/dvdy.21836.

Reznikov, N., Shahar, R., Weiner, S., 2014. Bone hierarchical structure in three dimensions. Acta Biomater. 10 (9), 3815–3826. https://doi.org/10.1016/j.actbio.2014.05.024.

Riedl, J., Crevenna, A.H., Kessenbrock, K., Yu, J.H., Neukirchen, D., Bista, M., Wedlich-Soldner, R., 2008. Lifeact: a versatile marker to visualize F-actin. Nat. Methods 5 (7), 605–607. https://doi.org/10.1038/nmeth.1220.

Shiflett, L.A., Tiede-Lewis, L.M., Xie, Y., Lu, Y., Ray, E.C., Dallas, S.L., 2019. Collagen dynamics during the process of osteocyte embedding and mineralization. Front. Cell Dev. Biol. 7, 178. https://doi.org/10.3389/fcell.2019.00178.

Sire, J.Y., Akimenko, M.A., 2004. Scale development in fish: a review, with description of sonic hedgehog (shh) expression in the zebrafish (Danio rerio). Int. J. Dev. Biol. 48 (2–3), 233–247. https://doi.org/10.1387/ijdb.15272389.

Sire, J.Y., Allizard, F., Babiar, O., Bourguignon, J., Quilhac, A., 1997. Scale development in zebrafish (Danio rerio). J. Anat. 190 (Pt 4), 545–561. https://doi.org/10.1046/j.1469-7580.1997.19040545.x.

Sun, S., Wang, Z., Hao, Y., 2008. Osterix overexpression enhances osteoblast differentiation of muscle satellite cells in vitro. Int. J. Oral Maxillofac. Surg. 37 (4), 350–356. https://doi.org/10.1016/j.ijom.2007.11.024.

Tsai, S.W., Hsu, Y.W., Pan, W.L., Vadivelmurugan, A., Hwang, P.A., Hsu, F.Y., 2022. Influence of the components and orientation of hydroxyapatite fibrous substrates on osteoblast behavior. J Funct Biomater 13 (4). https://doi.org/10.3390/jfb13040168.

Urasaki, A., Morvan, G., Kawakami, K., 2006. Functional dissection of the Tol2 transposable element identified the minimal cis-sequence and a highly repetitive sequence in the subterminal region essential for transposition. Genetics 174 (2), 639–649. https://doi.org/10.1534/genetics.106.060244.

Yu, S.M., Li, Y., Kim, D., 2011. Collagen mimetic peptides: progress towards functional applications. Soft Matter 7 (18), 7927–7938. https://doi.org/10.1039/C1SM05329A.

Zou, L., Zou, X., Li, H., Mygind, T., Zeng, Y., Lü, N., Bünger, C., 2006. Molecular mechanism of osteochondroprogenitor fate determination during bone formation. Adv. Exp. Med. Biol. 585, 431–441. https://doi.org/10.1007/978-0-387-34133-0_28.

Zuiderveld, K., 1994. Contrast limited adaptive histogram equalization. In: Heckbert, P.S. (Ed.), Graphics Gems IV. Academic Press Professional, Inc., San Diego, CA, USA, pp. 474–485. http://dl.acm.org/citation.cfm?id=180895.180940.

Zylberberg, L., Bereiter-Hahn, J., Sire, J.Y., 1988. Cytoskeletal organization and collagen orientation in the fish scales. Cell Tissue Res. 253 (3), 597–607. https://doi.org/10.1007/BF00219750.